

Plasmon tunability in metalodielectric metamaterials

Sampsa Riikonen,¹ Isabel Romero,¹ and F. J. García de Abajo^{1,2*}

¹*Donostia International Physics Center, Paseo Manuel de Lardizabal 4, 20018 San Sebastian, Spain*

²*Unidad de Física de Materiales CSIC-UPV/EHU Aptdo. 1072, 20080 San Sebastian, Spain*

(Dated: November 5, 2021)

The dielectric properties of metamaterials consisting of periodically arranged metallic nanoparticles of spherical shape are calculated by rigorously solving Maxwell's equations. Effective dielectric functions are obtained by comparing the reflectivity of planar surfaces limiting these materials with Fresnel's formulas for equivalent homogeneous media, showing mixing and splitting of individual-particle modes due to inter-particle interaction. Detailed results for simple cubic and fcc crystals of aluminum spheres in vacuum, silver spheres in vacuum, and silver spheres in a silicon matrix are presented. The filling fraction of the metal f is shown to determine the position of the plasmon modes of these metamaterials. Significant deviations are observed with respect to Maxwell-Garnett effective medium theory for large f , and multiple plasmons are predicted to exist in contrast to Maxwell-Garnett theory.

PACS numbers: 73.20.At, 71.10.Pm, 79.60.Jv, 81.07.Vb

I. INTRODUCTION

Artificial materials with tailored optical response functions (metamaterials) constitute a rich field of research due to their applicability to facilitate the design of highly-demanding optical devices for computing and communications technologies. That is the case of left-handed materials, which possess negative index of refraction¹ and permit designing lenses of resolution below the diffraction limit.² Furthermore, newly available nanostructured materials^{3,4,5,6} pose interesting possibilities that deserve detailed exploration to search for extraordinary optical properties.

Composite materials with components of dimensions much smaller than the light wavelength can be assimilated in general to equivalent homogeneous media with macroscopic optical properties such as a dielectric function and a magnetic permeability. The problem of finding the effective optical response of arrays of homogeneous spheres was already discussed by Maxwell.⁷ In fact, effective medium theories that yield simple analytical expressions have been available for nearly a century, like in the case of Maxwell-Garnett's theory (MGT),⁸ which is particularly suited to describe spherical inclusions and rather accurate at small concentrations of the latter f , or Bruggeman's theory,⁹ less accurate but intended to work for arbitrary values of f . Extensions and corrections to these theories have been reported over the last decades for periodic^{10,11,12,13,14,15,16,17,18,19,20,21,22} and disordered^{12,18,23,24,25,26,27} composites, all of them sharing in common the assumption of local response.

For metallic components plasmons are observed as collective oscillations of the valence electrons. In bulk metals, they are signalled by the vanishing of bulk dielectric function, $\epsilon = 0$. For an ideal metallic behavior as that described by Drude's formula

$$\epsilon(\omega) = 1 - \frac{\omega_p^2}{\omega(\omega + i\eta)}, \quad (1)$$

with $\eta \rightarrow 0^+$, this occurs at the bulk plasmon frequency $\omega = \omega_p$. The plasmon frequency is affected by the shape of the boundary of the metal, and for instance surface plasmons occur with frequency $\omega_s = \omega_p/\sqrt{2}$ at a planar surface, whereas modes of frequencies $\omega_l = \omega_p\sqrt{l/(2l+1)}$ are observed in spherical particles in the long-wavelength limit, corresponding to multipole oscillations of orders $l = 1, 2, \dots$, as described in the early work of Mie.²⁸ Multipolar plasmons can be also found in non-spherical metallic particles like nanorods,²⁹ nanorings,³⁰ and nanoshells.³¹ Collective modes in these particles and in particle pairs have been explained intuitively by invoking *plasmon chemistry* concepts following the general procedure outlined in Ref. 32. For layers of particles on a substrate, new plasmons are observed as a result of their mutual interaction.³³ In 3D periodic arrangements of spheres like the ones discussed below, Inglesfield *et al.*²¹ have reported a comprehensive study of plasmon bands and have found that wide bands do exist and that significant deviations from MGT occur in near-touching metal spheres. This connects to previous results on plasmon-like behavior in wired structures at THz frequencies.³⁴

In this work we concentrate on metamaterials formed by periodic arrays of metallic spherical nanoparticles confined within a host dielectric medium. We calculate their effective dielectric function from a rigorous solution of Maxwell's equations, therefore including all multipole corrections in an exact fashion, as a function of metallic filling fraction f . Tunable plasmons like the ones under study here can find application to light sensors, absorbers and emitters of light, and functional lasers.³⁵ The relevance of this study is illustrated by the several methods that have been developed for synthesizing nanocomposites, making use of nanoparticles self-assembly^{3,36,37,38} to prepare ordered layers of metallic particles in dielectric hosts, including fcc arrangements of Au particles in Si³⁸ and other complex particle shapes.^{4,5}

This paper shows how the plasma frequencies can be

engineered in metalodielectric composites consisting of spherical metallic nanoparticles embedded in a dielectric host. We consider in particular simple cubic (sc) and fcc arrays of aluminium nanoparticles in vacuum, as well as fcc arrays of silver nanoparticles surrounded by either vacuum or silicon. Modes other than dipolar are not resolved by external light in isolated nanoparticles, which leads to the prediction of a single plasmon branch as a function of metallic filling fraction when MGT is used. However, our rigorous solution of Maxwell's equations reveals several plasmon branches as a result of mixing and splitting of individual-particle modes of multipolar nature.

II. PLASMON CHEMISTRY

The basic ingredients of the composites under consideration are metallic nanoparticles. A isolated metallic nanoparticle can exhibit dipolar excitations with triple degeneracy (along the three orthogonal directions of space). When the dielectric function of the metal is described by Eq. (1), the frequency of these modes is $\omega_1 = \omega_p/\sqrt{3}$.³⁹ However, the interaction between neighboring nanoparticles can produce mixing and splitting of these dipolar modes, in a way similar to the mixing and splitting of p orbitals in molecular binding, which suggests the term of *plasmon chemistry*. The mode frequencies and their corresponding polarization patterns for two spheres of radius R interacting at a certain distance d are represented in Fig. 1, where the two intermediate frequency states are doubly degenerate. Of these modes, only the lowest lying one and the third one ($\omega_1\sqrt{1+R^3/d^3}$) display a net dipole moment, and therefore, external light with these two frequencies should couple strongly to this structure, whereas the other modes are either symmetry forbidden, depending on the light incidence conditions, or contribute very little to light scattering (silent modes).

These conclusions are corroborated by the scattering cross section represented in Fig. 2 for two small Al spheres as a function of light frequency and distance between the sphere centers d . Two different polarization directions have been considered, as shown in the insets. Results similar to those of Figs. 1 and 2 have been reported in Ref. 32.

The cross section is obtained by using the multiple elastic scattering of multipole expansions method (MESME), designed to solve Maxwell's equations in the presence of large numbers of particles in arbitrary positions.⁴⁰ In it, the electric field is expressed in frequency space ω in terms of magnetic and electric scalar functions ψ_i^M and ψ_i^E , respectively, as⁴¹

$$\mathbf{E} = \sum_i [\mathbf{L}_i \psi_i^M - \frac{1}{k} \nabla \times \mathbf{L}_i \psi_i^E],$$

where $k = \omega/c$, $\mathbf{L}_i = -i(\mathbf{r} - \mathbf{r}_i) \times \nabla$ is the orbital angular-momentum operator, the sum is extended over particle

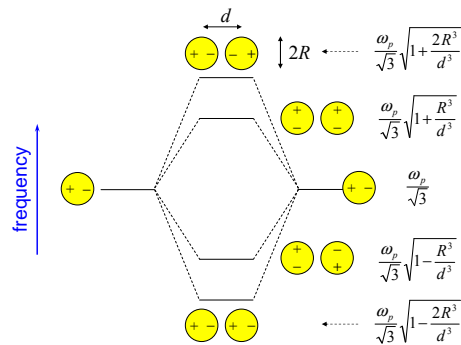


FIG. 1: Plasmon chemistry in interacting nanoparticles. The non-retarded plasmon energies of two identical metallic particles are shown along with schematic representations of the corresponding oscillation modes. The particles have radius R , their center-to-center distance is d , and the metal is described by a Drude dielectric function of bulk-plasma frequency ω_p [Eq. (1)]¹

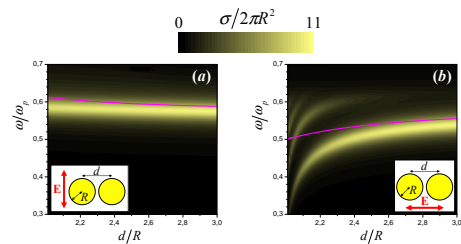


FIG. 2: Total scattering cross section σ of a system formed by two metallic spheres as a function of incident photon energy ω and center-to-center distance d between two aluminum spheres described by the Drude dielectric function of Eq. (1) with $\omega_p = 15$ eV and $\eta = 0.6$ eV. Two different polarization directions of the external electric field have been considered in (a) and (b), as shown in the insets. σ is normalized to the projected area of the two spheres, $2\pi R^2$. The solid curves represent the modes given by the expressions of Fig. 1.

positions \mathbf{r}_i , and M and E refer to magnetic and electric polarization, respectively. The electromagnetic field created by some external source is expanded in terms of spherical waves as

$$\psi_i^{\text{ext}}(\mathbf{r}) = \sum_{lm} i^l j_l(k|\mathbf{r} - \mathbf{r}_i|) Y_{lm}(\widehat{\mathbf{r} - \mathbf{r}_i}) \psi_{i,lm}^{\text{ext}},$$

where j_l is a spherical Bessel function, Y_{lm} is a spherical harmonic, and a polarization index (either magnetic or electric) is understood. In the absence of multiple scattering, the induced part of the scalar functions $\psi_i^{\text{ind}} = \psi_i^{\text{ss}}$ results from single scattering (ss) of ψ_i^{ext} by each object:

$$\psi_i^{\text{ss}}(\mathbf{r}) = \sum_{lm} i^l h_l^{(+)}(k|\mathbf{r} - \mathbf{r}_i|) Y_{lm}(\widehat{\mathbf{r} - \mathbf{r}_i}) \psi_{i,lm}^{\text{ss}}, \quad (2)$$

for \mathbf{r} outside the particle centered at \mathbf{r}_i . Here, $h_l^{(+)}$ is a spherical Hankel function. The relation between ψ_i^{ext} and ψ_i^{ss} is provided by the scattering matrix t_i , implicitly defined by $\tilde{\psi}_i^{\text{ss}} = t_i \tilde{\psi}_i^{\text{ext}}$, where $\tilde{\psi}_i^{\text{ss}(\text{ext})}$ is a vector

of components $\psi_{i,lm}^{\text{ss(ext)}}$. The matrix t_i describes the full scattering properties of object \mathbf{r}_i . In a cluster of several particles, ψ^{ind} takes the same form as Eq. (2), except that it is made up of ψ_i^{ss} (single scattering of the external field at \mathbf{r}_i) plus the result of the free propagation of ψ_j^{ind} from each object $\mathbf{r}_j \neq \mathbf{r}_i$, followed by scattering at \mathbf{r}_i (self-consistent multiple scattering). That is,⁴⁰

$$\tilde{\psi}_i^{\text{ind}} = \tilde{\psi}_i^{\text{ss}} + t_i \sum_{j \neq i} H_{ij} \tilde{\psi}_j^{\text{ind}}, \quad (3)$$

where the operator H_{ij} describes the noted propagation. In this work we consider homogeneous spheres, so that t_i becomes diagonal and given by analytical expressions.⁴⁰ Furthermore, we have found convergent results, using a finite number of multipoles with $l \leq 8$.

For a bi-sphere system, Fig. 2(b) demonstrates that only the lowest-frequency mode is excited for incident-light polarization along the inter-particle direction, whereas Fig. 2(a) shows that only the third hybridized dipolar mode contributes for polarization perpendicular to the inter-particle direction, as expected from the above discussion. The plasmon modes derived from the simple dipole-mode hybridization model of Fig. 1 follow the regions of large cross section only for relatively large values of d (solid curves in Fig. 2). Moreover, new resonances show up for parallel polarization [Fig. 2(b)] when the spheres are close together, as a result of stronger interaction among multipoles of the spheres that produce hybridized modes with net dipole moment along the external field direction.

In a structure formed by a distribution of small nanoparticles, one can use the Clausius-Mossotti formula⁴² that links the polarizability of the particles α to the effective dielectric function of such material ϵ_{eff} :

$$\frac{\epsilon_{\text{eff}} - \epsilon_h}{\epsilon_{\text{eff}} + 2\epsilon_h} = \frac{4\pi}{3} \frac{\alpha}{v}, \quad (4)$$

where v is the average volume per particle and ϵ_h is the dielectric function of the host material. This formula does not take into consideration non-dipolar interactions, and the effect of local order is neglected. However, it works quite well for small particle concentrations. The polarizability of metallic nanoparticles of radius R can be obtained as a function of the dielectric function of the metal ϵ_m as

$$\alpha = R^3 \epsilon_h \frac{\epsilon_m - \epsilon_h}{\epsilon_m + 2\epsilon_h}. \quad (5)$$

The combination of Eqs. (4) and (5) is equivalent to MGT.⁸ This theory predicts a single plasmon for the composite medium that obeys the relation

$$\epsilon_m = \frac{2(1-f)}{2+f} \epsilon_h \quad (6)$$

as a function of metal filling fraction $f = 4\pi R^3/3v$. Eq. (6) has been represented in Figs. 3 and 4 by solid curves.

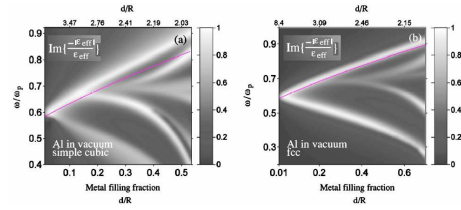


FIG. 3: Contour plot of $\text{Im}\{-|\epsilon_{\text{eff}}|/\epsilon_{\text{eff}}\}$ as a function of incident photon energy ω and filling fraction of the metal for

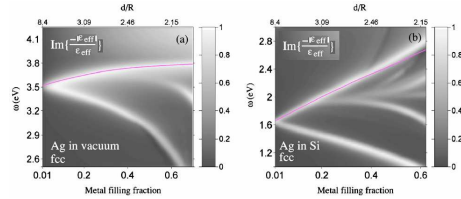


FIG. 4: Contour plot of $\text{Im}\{-|\epsilon_{\text{eff}}|/\epsilon_{\text{eff}}\}$ as a function of incident photon energy ω and filling fraction of the metal for silver spheres in an fcc configuration, surrounded by (a) vacuum or (b) silicon. Brighter regions correspond to higher values of $\text{Im}\{-|\epsilon_{\text{eff}}|/\epsilon_{\text{eff}}\}$. The solid curves correspond to Maxwell-Garnett theory as given by Eq. (6).

When the spheres are relatively close to each other, multipolar terms become relevant in the effective response, which are not accounted for by Eq. (6). Here, we have included them by rigorously solving Maxwell's equations using the MESME formalism sketched above and summarized in Eq. (3), as applied to periodic composites consisting of a large number of layers of nanoparticles. First, reflectance and transmittance matrices of incoming and scattered plane waves are obtained for each layer using a MESME-like procedure. Then, the interaction among layers is described by combining their reflectance and transmission matrices. More details about this so-called layer-KKR method, along with an efficient implementation, can be found in the excellent work of Stefanou *et al.*⁴³ We have followed their approach and have used less than 151 plane waves to obtain convergence in the examples that follow, with the largest number of waves needed when the spheres are nearly close-packed, as expected from previously reported divergence effects.⁴⁴

The effective dielectric function ϵ_{eff} is obtained by comparison of the reflectance coefficient of a surface of the composite materials under study to Fresnel's equations for equivalent homogeneous media.⁴² We have found that a single value of ϵ_{eff} can reproduce the angular dependence of the reflectance coefficients for all light polarizations with excellent numerical precision as long as the lattice period is small compared to the wavelength in the host material.

III. RESULTS AND DISCUSSION

We have applied the above formalism to study the following systems: periodic arrays of aluminum spheres placed in vacuum in simple cubic and fcc configurations (Fig. 3), and fcc arrays of silver spheres surrounded by either vacuum or silicon (Fig. 4). The dielectric constants of the materials under consideration have been taken from optical data.⁴⁵ In all cases, the distance between nearest neighbor sites has been taken as 6 nm, although our results are quite insensitive to the choice of this parameter, as long as it is much smaller than the wavelength.

Figures 3 and 4 show contour plots of the so-called loss function, $\text{Im}\{-1/\epsilon_{\text{eff}}\}$, illustrating its dependence on metal filling fraction f and light frequency. In the absence of absorption, the loss function diverges at the plasma frequencies ($\epsilon_{\text{eff}} = 0$), but in the actual, lossy systems under discussion this divergence is turned into finite peaks. Therefore, the regions of large values of the loss function (bright areas) correspond to plasmon excitations of the composites. Let us mention that the loss function inherits its name from the relevant role that it plays in electron energy loss spectroscopy (EELS), where it provides the loss spectrum for electrons traversing the bulk of a material.⁴⁶

Aluminum is a good example of a material where the Drude formula (1) describes extremely well its bulk dielectric function with the parameters given in the caption of Fig. 2. Therefore, we consider first a system of Al spheres in vacuum as a prototype system to study plasmon chemistry in metallic particle arrays. We observe that there are more than one plasmon for each value of the filling fraction, unlike the single plasmon prediction of Eq. (6) based upon MGT. The plasmon frequency derived from that formula (solid curves in Fig. 3) follows relatively well the highest-frequency plasmon of the rigorous calculation. This agreement is better in the fcc lattice [Fig. 3(b)]. However, this structure exhibit other plasmons that originate in the splitting and mixing of individual particle modes. These plasmon frequencies merge into the isolated particle limit $\omega_p/\sqrt{3}$ as $f \rightarrow 0$. For small values of f , there are only two plasmon branches that contribute significantly, arising from dipole-dipole interaction among the spheres, although the low-frequency branch is less clear in the simple cubic lattice. For larger f , new plasmon modes show up in the loss function as a result of interaction between multiples of higher order, in agreement with Ref. 21. This trend becomes dramatic near the percolation limit, where the material is expected to acquire good metallic behavior.^{47,48}

For an fcc array of Ag nanoparticles (Fig. 4), one can draw similar conclusions. When the host material is Si [Fig. 4(b)] the plasmon peaks are red shifted as compared to host vacuum [Fig. 4(a)] and the plasmon peaks are relatively more spaced in frequency for a given value of f . Metallic nanoparticles embedded in Si constitute systems that have become recently realizable in practice,³⁸ so that

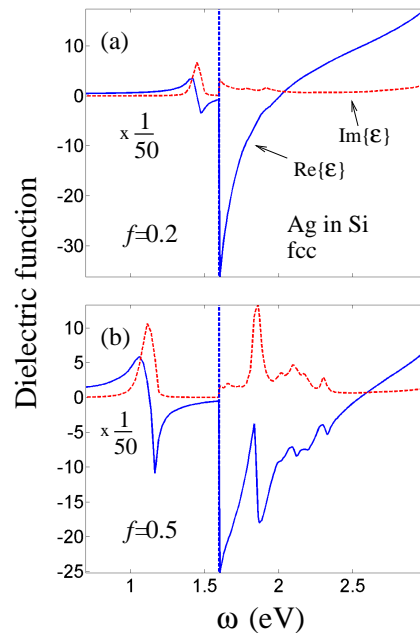


FIG. 5: Real and imaginary parts of the effective dielectric function ϵ_{eff} for an fcc arrangement of Ag spheres surrounded by Si (solid and broken curves, respectively). Two different filling fractions of the metal have been considered: (a) $f = 0.2$ and (b) $f = 0.5$. The dielectric function has been divided by 50 in the low- ω region to improve readability.

the results presented here bear predictions that can be addressed experimentally.

Both real and imaginary parts of the dielectric function have been represented in Fig. 5 for fcc lattices of Ag spheres in Si and with different values of the metal filling fraction ($f = 0.2$ and $f = 0.5$). This figure indicates that the highest-energy plasmon branch observed in Fig. 4(b) arises from the vanishing of the real part of ϵ_{eff} , with no further features showing up in the imaginary part, which is consistent with the fact that this plasmon is relatively close to the single plasmon predicted by MGT. This is quite different from the lowest-energy plasmon, where ϵ_{eff} itself exhibits a resonant behavior translated into a Lorentzian-type shape, including a peak in the imaginary part. Other resonances of multipolar origin at intermediate energies [see Fig. 4(b)] are mainly associated to peaks in the imaginary part, which are particularly clear in Fig. 5(b) for $f = 0.5$. Our calculations for the rest of the combinations of lattice, metal, and embedding material considered in this work allow us to draw a similar picture in those cases.

In conclusion, we have shown that the plasmons exhibited by metallic nanoparticles do hybridize when the particles are close to each other, and this produces new plasmon modes whose frequency can be tuned by changing the distance between the particles. This suggests the possibility of designing temperature and pressure sensors based upon changes in the plasmon frequency with small

variations of the filling fraction, particularly near the percolation limit (e.g., using short thiols to coat the particles in order to have small separations between them). Our study demonstrates the failure of Maxwell-Garnett theory,^{8,18} that predicts only a single plasmon in these structures, rather than the rich structure of plasmons revealed by our rigorous solution of the full electromagnetic problem, not to mention Bruggeman's theory,^{9,18} that does not predict a plasmon at all.⁴⁹

Acknowledgments

FJGA would like to thank F. Meseguer, M. Käll, J. M. Pitarke, and J. Fernández for helpful discus-

sions. This work was supported by the University of the Basque Country UPV/EHU (contract No. 00206.215-13639/2001), by the late Spanish Ministerio de Ciencia y Tecnología and the new Ministerio de Educación y Ciencia (contract Nos. MAT2001-0946 and FIS2004-06490-C03-02, respectively), and by the European Union (*Metamorphose* Network of Excellence, NMP3-CT-2004-500252). SR was partially supported by the Emil Aaltonen Foundation.

* Corresponding author.

- ¹ R. A. Shelby, D. R. Smith, and S. Schultz, *Science* **292**, 77 (2001).
- ² J. B. Pendry, *Phys. Rev. Lett.* **85**, 3966 (2000).
- ³ T. Ung, L. M. Liz-Marzán, and P. Mulvaney, *J. Phys. Chem.* **105**, 3441 (2001).
- ⁴ F. Caruso, M. Spasova, V. Salgueirio-Maceira, and L. M. Liz-Marzán, *Adv. Mater.* **13**, 1090 (2001); L. M. Liz-Marzán and P. Mulvaney, *J. Phys. Chem. B* **107**, 7312 (2003).
- ⁵ V. F. Puentes, K. M. Krishnan, and A. P. Alivisatos, *Science* **291**, 2115 (2001).
- ⁶ Y. Ding, Y. Kim, and J. Erlebacher, *Adv. Mater.* **16**, 1897 (2004).
- ⁷ J. C. Maxwell, *Electricity and Magnetism* (Oxford, Clarendon, 1873).
- ⁸ J. C. Maxwell-Garnett, *Philos. Trans. R. Soc. London A* **203**, 385 (1904); **205**, 237 (1906).
- ⁹ D. A. G. Bruggeman, *Ann. Phys. (Leipzig)* **24**, 636 (1935).
- ¹⁰ D. J. Bergman, *Phys. Rev. B* **19**, 2359 (1979).
- ¹¹ P. Sheng, *Phys. Rev. Lett.* **45**, 60 (1980).
- ¹² W. Lamb, D. M. Wood, and N. W. Ashcroft, *Phys. Rev. B* **21**, 2248 (1980).
- ¹³ G. W. Milton, *Appl. Phys. A* **26**, 1207 (1981).
- ¹⁴ R. Tao, Z. Chen, and P. Sheng, *Phys. Rev. B* **41**, 2417 (1990).
- ¹⁵ D. J. Bergman and K.-J. Dunn, *Phys. Rev. B* **45**, 13262 (1992).
- ¹⁶ S. Datta, C. T. Chan, K. M. Ho, and C. M. Soukoulis, *Phys. Rev. B* **48**, 14936 (1993).
- ¹⁷ L. Martín-Moreno and J. B. Pendry, *Nucl. Instrum. Methods Phys. Res. B* **96**, 565 (1995).
- ¹⁸ W. Lü, J. Dong, and Z.-Y. Li, *Phys. Rev. B* **63**, 33401 (2000).
- ¹⁹ Z. Liu, C. T. Chan, P. Sheng, A. L. Goertzen, and J. H. Page, *Phys. Rev. B* **62**, 2446 (2000).
- ²⁰ H. Ma, B. Zhang, W. Y. Tam, and P. Sheng, *Phys. Rev. B* **61**, 962 (2000).
- ²¹ J. E. Inglesfield, J. M. Pitarke, and R. Kemp, *Phys. Rev. B* **69**, 233103 (2004).
- ²² F. J. García de Abajo and L. A. Blanco, *Phys. Rev. B* **67**, 125108 (2003).
- ²³ R. I. Cukier, J. Karkheck, S. Kumar, and S. Y. Sheu, *Phys. Rev. B* **41**, 1630 (1990).
- ²⁴ S.-Y. Sheu, S. Kumar, and R. I. Cukier, *Phys. Rev. B* **42**, 1431 (1990).
- ²⁵ K. Hinsén and B. U. Felderhof, *Phys. Rev. B* **46**, 12955 (1992).
- ²⁶ R. G. Barrera and R. Fuchs, *Phys. Rev. B* **52**, 3256 (1995).
- ²⁷ C. Noguez and R. G. Barrera, *Phys. Rev. B* **57**, 302 (1998).
- ²⁸ G. Mie, *Ann. Phys.* **25**, 377 (1908).
- ²⁹ J. R. Krenn, G. Schider, W. Rechberger, B. Lamprecht, A. Leitner, and F. R. Ausseneg, *Appl. Phys. Lett.* **77**, 3379 (2000).
- ³⁰ J. Aizpurua, P. Hanarp, D. S. Sutherland, M. Käll, G. W. Bryant, and F. J. García de Abajo, *Phys. Rev. Lett.* **90**, 057401 (2003).
- ³¹ E. Prodan, C. Radloff, N. J. Halas, and P. Nordlander, *Science* **302**, 419 (2003).
- ³² P. Nordlander, C. Oubre, E. Prodan, K. Li, and M. I. Stockman, *Nano Lett.* **4**, 899 (2004).
- ³³ A. Taleb, V. Russier, A. Courty, and M. P. Pileni, *Phys. Rev. B* **59**, 13350 (1999).
- ³⁴ J. B. Pendry, A. J. Holden, W. J. Stewart, and I. Youngs, *Phys. Rev. Lett.* **76**, 4773 (1996).
- ³⁵ V. C. Sundar, H. J. Eisler, and M. G. Bawendi, *Adv. Mater.* **14**, 739 (2002).
- ³⁶ M. Gadenne, V. Podolskiy, P. Gadenne, P. Sheng, and V. M. Shalaev, *Europhys. Lett.* **53**, 364 (2001).
- ³⁷ D. Zanchet, M. S. Moreno, and D. Ugarte, *Phys. Rev. Lett.* **82**, 5277 (1999).
- ³⁸ H. Fan, K. Yang, D. M. Boye, T. Sigmon, K. J. Malloy, H. Xu, G. P. López, and C. J. Brinker, *Science* **304**, 567 (2004).
- ³⁹ Here, we work in the electrostatic limit, but the plasma fre-

- quencies of spheres comparable in size to the wavelength are generally red-shifted, as demonstrated via electron-induced light emission experiments using an electron microscope in N. Yamamoto, K. Araya, and F. J. García de Abajo, Phys. Rev. B **64**, 205419 (2001).
- ⁴⁰ F. J. García de Abajo, Phys. Rev. Lett. **82**, 2776 (1999); Phys. Rev. B **60**, 6086 (1999).
- ⁴¹ F. E. Low, *Classical Field Theory: Electromagnetism and Gravitation* (John Wiley & Sons, New York, 1997).
- ⁴² J. D. Jackson, *Classical Electrodynamics* (Wiley, New York, 1975).
- ⁴³ N. Stefanou, V. Yannopoulos, and A. Modinos, Comput. Phys. Commun. **113**, 49 (1998); **132**, 189 (2000).
- ⁴⁴ A. Pack, M. Hietschold, and R. Wannemacher, Opt. Comm. **194**, 277 (2001).
- ⁴⁵ E. D. Palik, *Handbook of Optical Constants of Solids* (Academic Press, New York, 1985).
- ⁴⁶ D. W. McComb and A. Howie, Ultramicroscopy. **34**, 84 (1990); Nucl. Instrum. Methods Phys. Res. B **96**, 569 (1995).
- ⁴⁷ C. Pecharromás and J. S. Moya, Adv. Mater. **12**, 294 (2000).
- ⁴⁸ C. Pecharromás, F. Esteban-Betegón, J. F. Bartolomé, S. López-Esteban, and J. S. Moya, Adv. Mater. **13**, 1541 (2001).
- ⁴⁹ Bruggeman's theory leads to an inequality when one imposes $\epsilon_{\text{eff}} = 0$.